Organic & Biomolecular Chemistry

www.rsc.org/obc

Volume 6 | Number 13 | 7 July 2008 | Pages 2217–2444

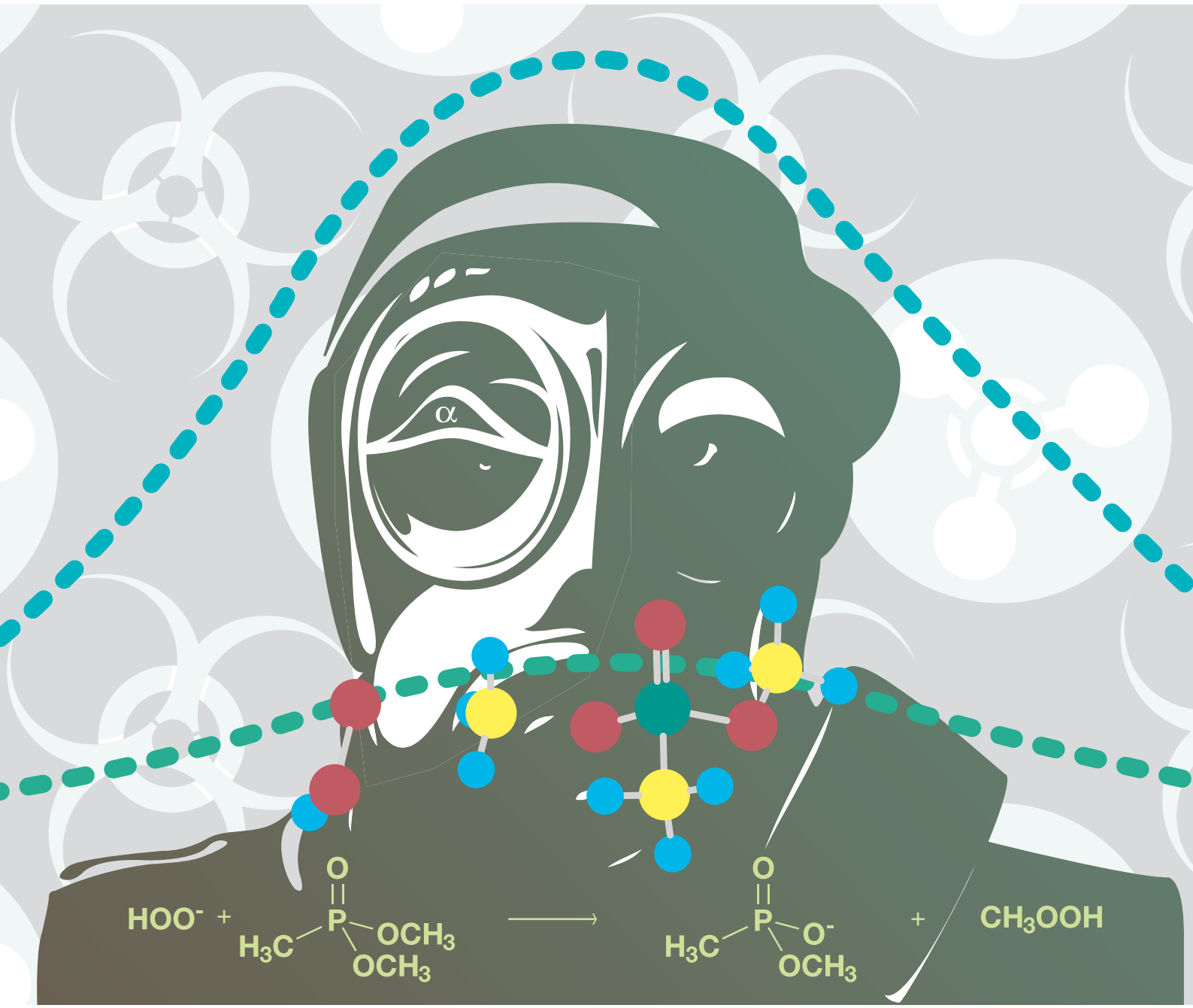

ISSN 1477-0520

RSC Publishing

Reactions of the hydroperoxide anion with dimethyl methylphosphonate in an ion trap mass spectrometer: evidence for a gas phase α-effect†

Andrew Michael McAnoy,*[a] Martin Robert Lloyd Paine[b] and Stephen James Blanksby*[b]

Received 4th March 2008, Accepted 2nd April 2008
First published as an Advance Article on the web 30th April 2008
DOI: 10.1039/b803734e

The gas phase degradation reactions of the chemical warfare agent (CWA) simulant, dimethyl methylphosphonate (DMMP), with the hydroperoxide anion (HOO^-) were investigated using a modified quadrupole ion trap mass spectrometer. The HOO^- anion reacts readily with neutral DMMP forming two significant product ions at *m/z* 109 and *m/z* 123. The major reaction pathways correspond to (i) the nucleophilic substitution at carbon to form $[CH_3P(O)(OCH_3)O]^-$ (*m/z* 109) in a highly exothermic process and (ii) exothermic proton transfer. The branching ratios of the two reaction pathways, 89% and 11% respectively, indicate that the former reaction is significantly faster than the latter. This is in contrast to the trend for the methoxide anion with DMMP, where proton transfer dominates. The difference in the observed reactivities of the HOO^- and CH_3O^- anions can be considered as evidence for an α-effect in the gas phase and is supported by electronic structure calculations at the B3LYP/aug-cc-pVTZ//B3LYP/6-31+G(d) level of theory that indicate the S_N2(carbon) process has an activation energy 7.8 kJ mol^{-1} lower for HOO^- as compared to CH_3O^-. A similar α-effect was calculated for nucleophilic addition–elimination at phosphorus, but this process – an important step in the perhydrolysis degradation of CWAs in solution – was not observed to occur with DMMP in the gas phase. A theoretical investigation revealed that all processes are energetically accessible with negative activation energies. However, comparison of the relative Arrhenius pre-exponential factors indicate that substitution at phosphorus is not kinetically competitive with respect to the S_N2(carbon) and deprotonation processes.

Introduction

Over recent years, the threat of chemical warfare agents (CWAs) has driven the development of enhanced methods for their detection and decontamination.[1] It has long been known that peroxide-based decontaminants effectively degrade CWAs,[2–4] and recent efforts in the development of environmentally benign decontamination technologies have led to an effective decontaminant which consists of hydrogen peroxide and a peroxide activator in solution.[5] The application of hydrogen peroxide in the vapour phase has also been shown to be effective against CWAs, allowing for the rapid remediation of contaminated buildings.[6] Interestingly, hydrogen peroxide alone in solution degrades isopropyl methyl phosphonofluoridate (GB) very slowly with a half-life measured by ^{31}P NMR in the order of days, while the degradation of GB with an activated hydrogen peroxide solution occurs too rapidly to measure by NMR.[5] In some instances the perhydrolysis reactions are between 40 and 300 times faster than the analogous alkaline hydrolysis or neutral oxidation processes.[4,7] Such observations are generally attributed to the increased nucleophilicity of the hydroperoxide anion due to the presence of a lone pair of electrons on the atom adjacent to the nucleophilic centre: a phenomenon often referred to as the 'α-effect'.[8] The peroxide anion has also been shown to selectively degrade *O*-ethyl *S*-[2-(diisopropylamino)ethyl] methylphosphonothioate (VX) to the non-toxic product ethyl methylphosphonic acid (EMPA).[3,4] The exclusive P–S cleavage reaction observed during the alkaline perhydrolysis of VX (Scheme 1) is a significant advantage over VX hydrolysis that can undergo P–S or P–O cleavage, with the latter process resulting in the formation of the toxic by-product *S*-[2-(diisopropylamino)ethyl] methylphosphonthioic acid (EA-2192).

The perhydrolysis reaction is generally regarded to proceed *via* a pentavalent intermediate, and a number of theoretical studies into the mechanism of the process have been reported.[9,10] For example, a recent theoretical study compared the alkaline perhydrolysis of a model VX compound to the analogous hydrolysis process and found that both reactions proceed *via* a phosphorus-centred pentavalent intermediate.[10] However, while reactions resulting in the cleavage of both P–O and P–S bonds of VX are kinetically competitive during hydrolysis, P–S bond cleavage was calculated to be kinetically favoured during alkaline perhydrolysis and explains the absence of the toxic product (*cf.* Scheme 1). Theoretical studies also indicate that a stable pentavalent intermediate is formed in the hydrolysis of the G-series of chemical agents.[10,11] While no pentavalent intermediates of CWAs have been observed directly, peroxy intermediates $[HOOP(O)(CH_3)OR$,

[a]*Human Protection and Performance Division, Defence Science and Technology Organisation, 506 Lorimer St, Fishermans Bend, Victoria, 3207, Australia. E-mail: andrew.mcanoy@dsto.defence.gov.au; Fax: +61 3 9626 8342; Tel: +61 3 9626 8414*
[b]*School of Chemistry, University of Wollongong, Wollongong, New South Wales, 2522, Australia. E-mail: blanksby@uow.edu.au; Fax: +61 2 4221 4287; Tel: +61 2 4221 5484*

† Electronic supplementary information (ESI) available: Vibrational partition functions; standard orientations for stationary points. See DOI: 10.1039/b803734e

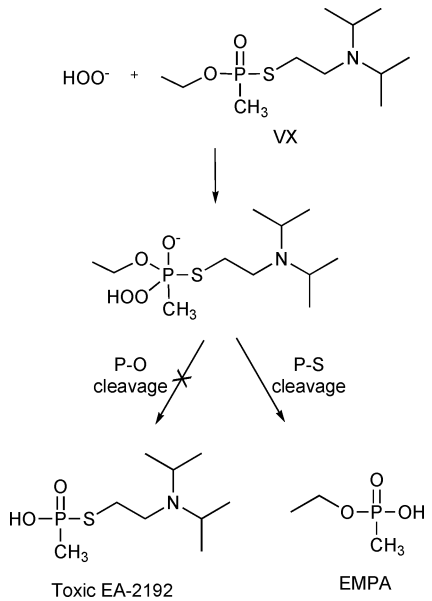

Scheme 1

R = $(CH_3)_2CH$, $(CH_3)_3CCH(CH_3)$] have been observed by ^{31}P NMR during the alkaline perhydrolysis of GB and pinacolyl methyl phosphonofluoridate (GD), and are consistent with nucleophilic attack at the phosphorus centre.[5]

The gas phase ion–molecule reactions of various anions with a number of organophosphorus compounds have been investigated using mass spectrometry.[12,13] In particular, Lum and Grabowski reported the gas phase reactions between selected anions and a CWA simulant, dimethyl methylphosphonate (DMMP). The reaction of the HO^- anion with DMMP resulted in almost exclusive deprotonation, while the F^- anion reacted by nucleophilic attack at both carbon and phosphorus centres.[13] This difference was suggested to be partly due to the enhanced nucleophilicity of the F^- ion toward the phosphorus centre. Interestingly, no study has been reported on the gas phase reactions between the HOO^- anion and organophosphorus compounds. Previous experimental work by DePuy *et al.* suggested that the nucleophilicity of peroxide anions in the gas phase is similar to that of hydroxide ions, indicating that the α-effect is not significant in the absence of solvent.[14] However, recent computational studies comparing anions of similar proton affinities indicate that α-nucleophiles have lower activation energies for nucleophilic substitution reactions at saturated carbon centres.[15] Further, α-nucleophiles with hard α-atoms, such as HOO^-, have a greater reduction in activation energy than those with soft α-atoms, such as BrO^-.[15] Therefore, in the absence of solvent effects, the study of gas phase reactions may provide insight into the intrinsic increase in nucleophilicity due to the α-effect. For example, does HOO^- undergo analogous reactions with DMMP as those observed for HO^-, or, does the increased nucleophilicity of HOO^- influence the reactivity toward substitution reactions as observed with F^-?

Here we describe experiments using a quadrupole ion trap mass spectrometer, modified to allow for the introduction of gaseous neutral reagents directly into the ion trap, to probe the reactions of F^-, CD_3O^- and HOO^- with neutral DMMP. The experimental results are complemented by hybrid density functional theory (DFT) calculations to elucidate mechanisms and determine relative energies of, and barriers to, pertinent reaction products and intermediates.

Results and discussion

Mass spectrometry

A general scheme for the reactions of various anions with neutral DMMP reported by Lum and Grabowski is shown in Scheme 2.[13] The major reaction pathways observed for each anion studied were deprotonation and nucleophilic substitution at ester carbons as determined by the observation of $[CH_2P(O)(OCH_3)_2]^-$ (*m/z* 123) and $[CH_3P(O)(OCH_3)O]^-$ (*m/z* 109), respectively. The addition of the reactant anion with loss of methanol is proposed as evidence for an active addition–elimination mechanism at phosphorus; for example, F^- was found to react with DMMP to form $[F(CH_3)P(O)OCH_3]^-$ (*m/z* 111). The final reaction process, observed to a minor extent for the NH_2^- anion only, was reductive elimination across a C–O bond. Interestingly, while the branching ratios were observed to be dependent on the incipient anion, the $[CH_2P(O)(OCH_3)_2]^-$ (*m/z* 123) product ion was observed to dominate whenever the deprotonation reaction channel was active.[13]

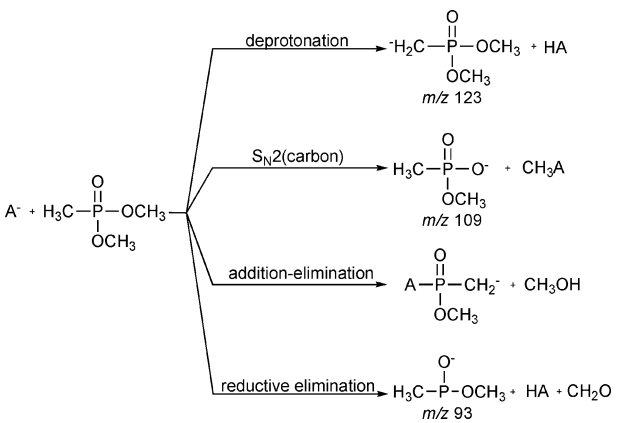

Scheme 2

The major product ion for the gas phase reaction of HO^- with DMMP was a result of the deprotonation process, with a branching ratio determined to be 96%. The S_N2(carbon) process was observed with a branching ratio of only 4%. This was similar to the gas phase reactions of the CD_3O^- ion with DMMP which were also dominated by deprotonation (93%), with addition–elimination at phosphorus (4%) and nucleophilic substitution at ester carbons (3%) occurring to only a minor extent. The proton affinities of HOO^- (1575 kJ mol^{-1})[16] and CH_3O^- (1597 kJ mol^{-1})[17] are similar, and both are greater than the proton affinity of DMMP (1560 kJ mol^{-1}).[13] Therefore, in the absence of a significant difference in gas phase nucleophilicities, the deprotonation process may be expected to similarly dominate for the reaction between HOO^- and DMMP. In contrast, the deprotonation pathway is switched off for the potent nucleophile F^- (PA = 1554 kJ mol^{-1}),[18] which reportedly undergoes nucleophilic substitution at the ester carbon (84%) and addition–elimination at the phosphorus centre (16%).[13]

Our interest in the intrinsic chemistry of the alkaline perhydrolysis of organophosphonates incited us to investigate the gas phase reactions of F^-, CD_3O^- and HOO^- with DMMP to (i) compare results with previous afterglow reactions, (ii) investigate the intrinsic differences between the alkaline hydrolysis and perhydrolysis of organophosphorus compounds using CH_3O^- as a surrogate for HO^-, and (iii) probe the existence of the α-effect in the gas phase. Product ion mass spectra for the reaction of DMMP with each of the anions are shown in Fig. 1. In addition, the product ion branching ratios for each of the reactions were determined using the Grabowski method, as described previously.[19]

Reactions of the F^- anion and evidence for a pentavalent intermediate. The F^- anion (*m/z* 19) was generated in the ion-source *via* electrospray ionisation of an aqueous solution of caesium fluoride. DMMP was injected into a heated inlet where it was volatilised and mixed with the helium buffer gas before being introduced into the ion trap and allowed to react with the isolated F^- anion. After a set reaction time, the product ions and remaining F^- ions were scanned out of the trap and detected. The major product ions in the resulting mass spectrum (Fig. 1a) correspond to the S_N2(carbon) and addition–elimination(phosphorus) products. The product ion which corresponded to deprotonated DMMP (*m/z* 123) was not significant and only observed in trace amounts. The branching ratio plot of product ion intensities against the consumption of the reactant ion is shown in Fig. 2. The branching ratios for the reactions are determined from the slopes to be 91% for the S_N2(carbon) process and 9% for the addition–elimination process, and are close agreement with reported branching ratios of 84% and 16% respectively.[13]

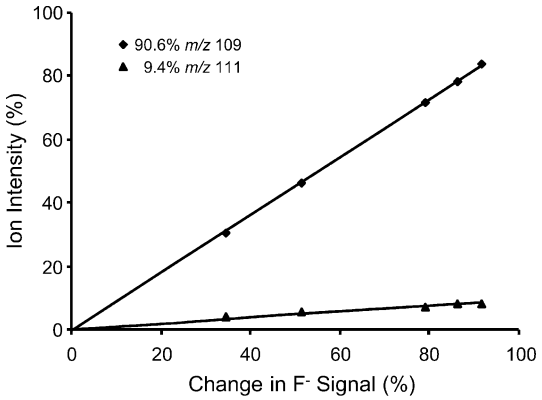

Fig. 2 Branching ratio plot observed for the reaction between F^- (*m/z* 19) and DMMP (124 Da) with a reaction time of 0.03 ms. MS experiments were conducted using a modified quadrupole ion trap mass spectrometer operating at a temperature of 307 K and pressure of 2.5 mTorr. The slopes afford branching ratios for the product ions *m/z* 109 (91%) and *m/z* 111 (9%).

The pentavalent intermediate for the F^- anion would be expected at *m/z* 143, and the absence of this ion in Fig. 1a indicates that the pentavalent intermediate is not stable under the reaction conditions and readily undergoes loss of methanol

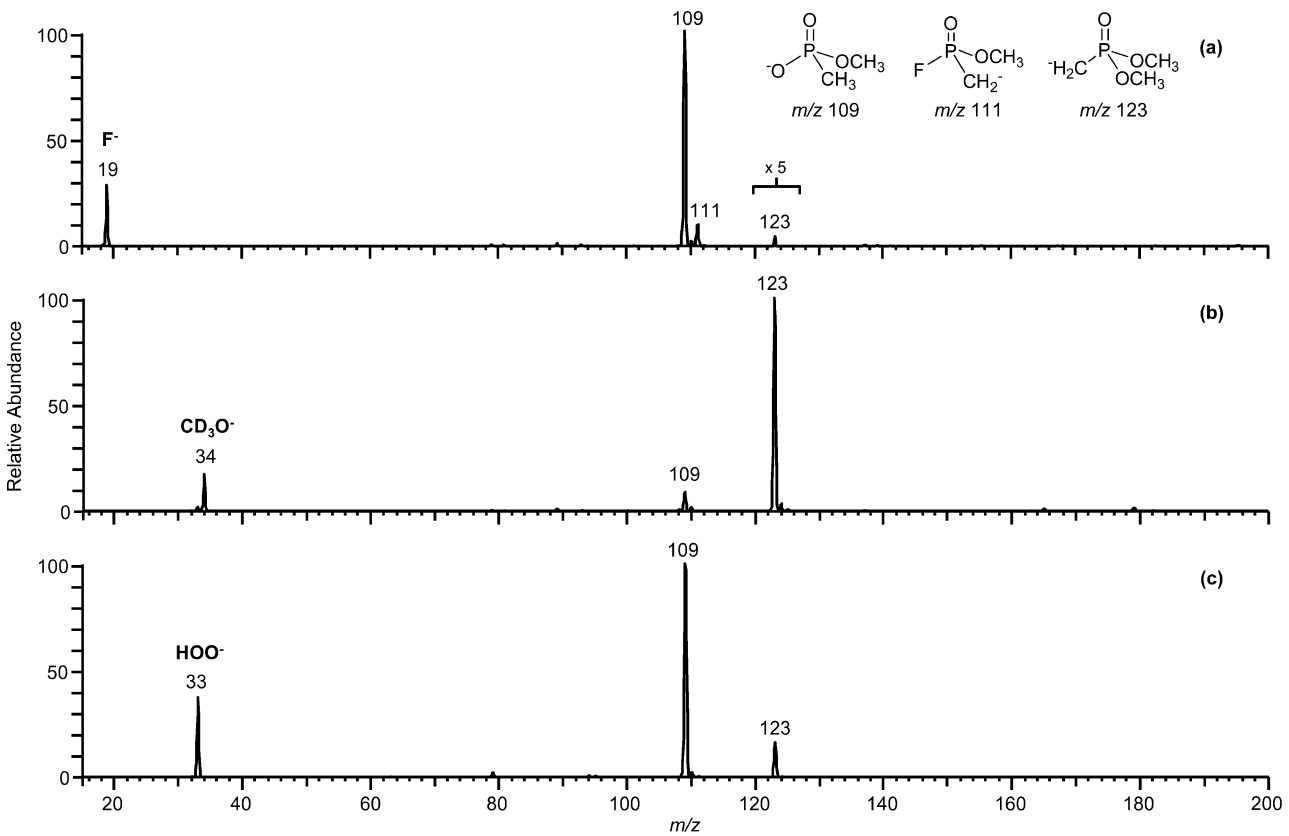

Fig. 1 Product ion spectra resulting from the gas phase reaction of (a) F^- (*m/z* 19) (b) CD_3O^- (*m/z* 34) and (c) HOO^- (*m/z* 33) with neutral DMMP. Product ions observed result from deprotonation (*m/z* 123), nucleophilic substitution at carbon (*m/z* 109) and addition–elimination at phosphorus (*m/z* 111).

to form the observed product ion at m/z 111. Interestingly, an ion at m/z 143 was observed in the full ESI MS spectrum under the reaction conditions and was not observed in the absence of DMMP. In this experiment, all ions generated in the ion source are available to react with neutral DMMP in the ion trap. As the m/z 143 ion is not observed during reaction of isolated F^- with DMMP (Fig. 1a), the only other evident source of F^- available to react with DMMP is the hydrated F^- ion, $[H_2O\cdots F]^-$ (m/z 37). The reaction of isolated $[H_2O\cdots F]^-$ with DMMP resulted in a major product ion at m/z 143 and a minor product ion at m/z 109 (Fig. 3a). Collision-induced dissociation (CID) of the m/z 143 product ion yielded fragment ions at m/z 109 and m/z 111 (Fig. 3b) with no evidence for the direct dissociation to F^- (m/z 19). The observed ions correspond to the S_N2(carbon) and addition–elimination(phosphorus) product ions respectively and thus the m/z 143 ion is consistent with the elusive pentavalent intermediate, $[F(CH_3)P(O)(OCH_3)_2]^-$. In this case, the reactive pentavalent intermediate formed by reaction of the hydrated F^- ion with DMMP is stabilised by the release of excess energy as translational energy of the departing H_2O neutral.

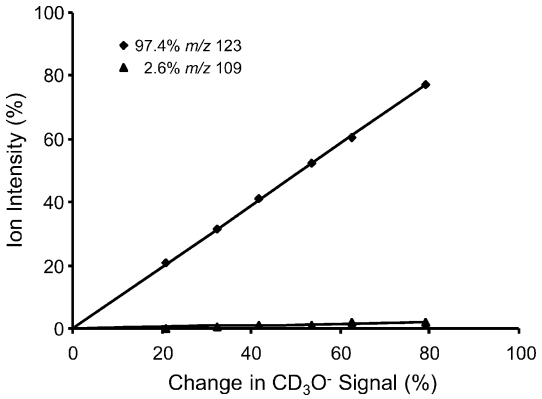

Fig. 4 Branching ratio plot observed for the reaction between CD_3O^- (m/z 34) and DMMP (124 Da) with a reaction time of 100 ms. MS experiments were conducted using a modified quadrupole ion trap mass spectrometer operating at a temperature of 307 K and pressure of 2.5 mTorr. The slopes afford branching ratios for the product ions m/z 123 (97%) and m/z 109 (3%).

Reactions of the CD_3O^- anion. The CD_3O^- anion (m/z 34) was isolated and allowed to react with neutral DMMP in the ion trap. The resulting product ion spectrum is shown in Fig. 1b and the plot of product ion intensities against the consumption of the reactant ion used to obtain branching ratios is shown in Fig. 4. The observed processes for the reaction between CD_3O^- and DMMP were deprotonation (97%) and the S_N2(carbon) pathway (3%) and are reasonably consistent with previously reported branching ratios of 93% and 3%.[13] In this experiment, the probe for the addition–elimination pathway is formation of an ion at m/z 126, $[CD_3O(CH_3)P(O)OCH_3]^-$, or an ion corresponding to the pentavalent intermediate at m/z 158. Thus, the absence of these ions in Fig. 1b indicates this process, observed to a minor extent (4%) in flowing afterglow experiments,[13] is not significant under ion trap conditions. This minor discrepancy between experiments, may arise from the significantly different pressure regimes of the two instruments used to observe this chemistry (flowing afterglow 0.3 Torr *versus* ion trap pressures of 2.5×10^{-3} Torr).

Reactions of the HOO^- anion. The HOO^- anion (m/z 33) was isolated and allowed to react with neutral DMMP in the ion trap. The major product ions observed in the resulting product ion mass spectrum (Fig. 1c) are consistent with expected reaction products of the S_N2(carbon) pathway to form the $[CH_3P(O)(OCH_3)O]^-$ ion at m/z 109 and the deprotonation pathway to form the $[CH_2P(O)(OCH_3)_2]^-$ ion at m/z 123. The plot of product ion intensities against the consumption of the hydroperoxide anion (Fig. 5) was used to determine the respective branching ratios of 89% and 11% for these processes. The characteristic addition–elimination product ion for the HOO^- anion would be expected at m/z 125 and an ion corresponding to the pentavalent intermediate at m/z 157, and thus the absence of these ions in Fig. 1c

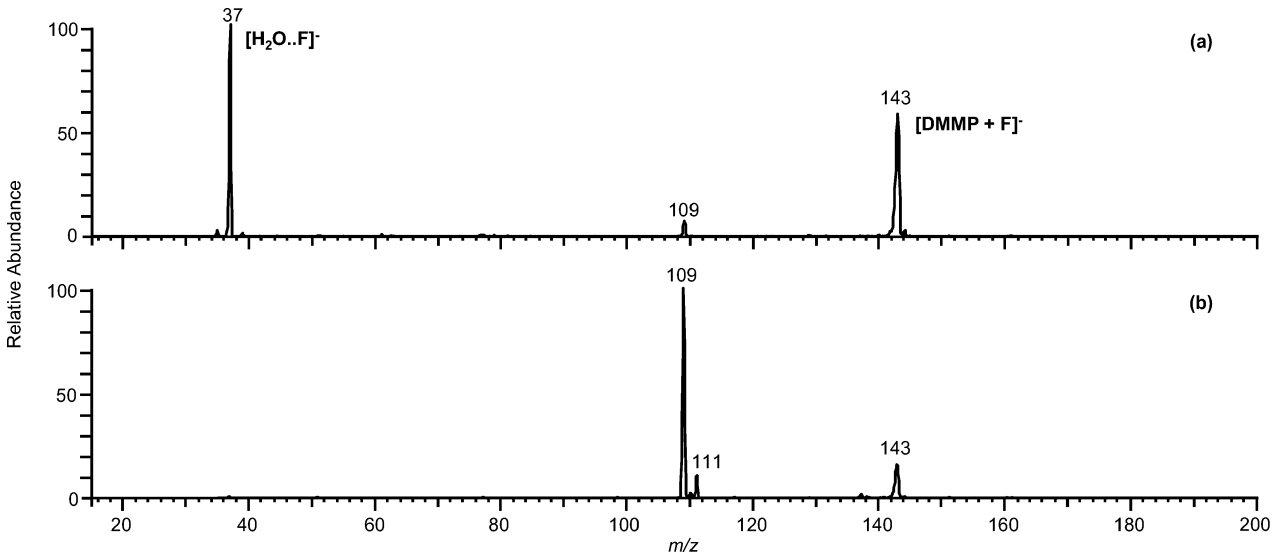

Fig. 3 (a) Product ion spectra observed for the reaction between $[H_2O\cdots F]^-$ (m/z 37) and DMMP (124 Da) and (b) CID spectrum of the resulting m/z 143 product ion, consistent with a pentavalent intermediate.

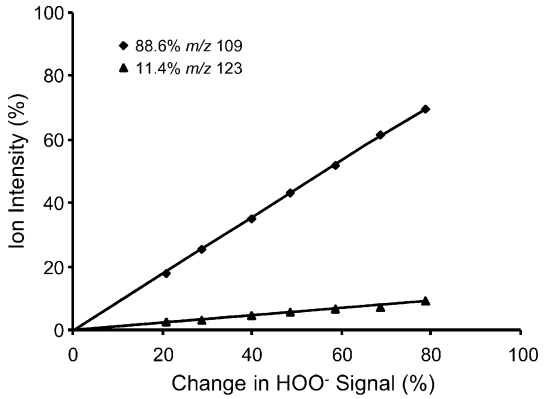

Fig. 5 Branching ratio plot observed for the reaction between HOO^- (m/z 33) and DMMP (124 Da) with a reaction time of 200 ms. MS experiments were conducted using a modified quadrupole ion trap mass spectrometer operating at a temperature of 307 K and pressure of 2.5 mTorr. The slopes afford branching ratios for the product ions m/z 109 (89%) and m/z 123 (11%).

indicates that HOO^- does not undergo any significant nucleophilic addition–elimination at phosphorus.

MS^n characterisation of observed product ions m/z 109 and m/z 123. The observed product ions at m/z 109 and m/z 123 are formed as a result of demethylation and deprotonation of DMMP. In each case the resulting product ion is resonance stabilised with the charge distributed to the phosphonyl oxygen as shown in Scheme 3 for the reaction of HOO^- (m/z 33) with neutral DMMP (124 Da).

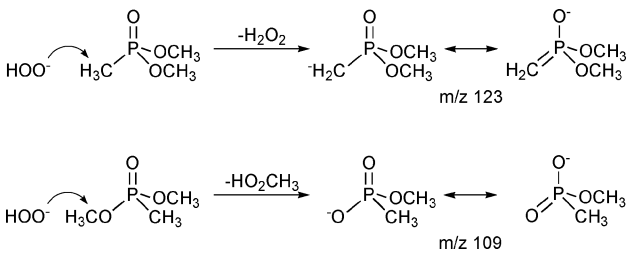

Scheme 3

The m/z 109 and m/z 123 product ions were characterised using MS^n experiments. CID of the m/z 33 → 109 ion yielded two significant fragment ions at m/z 77 and m/z 94, which correspond to a loss of CH_3OH and $^{\bullet}CH_3$ respectively (Fig. 6a). This is consistent with the proposed $[CH_3P(O)(OCH_3)O]^-$ structure of the m/z 109 product ion (Scheme 3). The neutral loss of CH_3OH involves simple heterolytic cleavage of a P–OCH_3 bond to generate a CH_3O^- ion-neutral complex, followed by deprotonation at the acidic CH_3P moiety to form the m/z 77 fragment ion, while the radical loss of $^{\bullet}CH_3$ forms a resonance-stabilised radical anion (Scheme 4).

The CID spectrum of the m/z 33 → 123 product ion (Fig. 6b) shows a major fragment ion at m/z 93 consistent with an ion formed by loss of formaldehyde. This MS^3 fragment ion (m/z 93) was further isolated and collisionally activated in an MS^4 experiment (Fig. 6c). An ion at m/z 78 was observed as the major fragment ion in the resulting MS^4 spectrum of the m/z 33 → 123 → 93 ion. This neutral loss of 15 Da corresponds to a radical

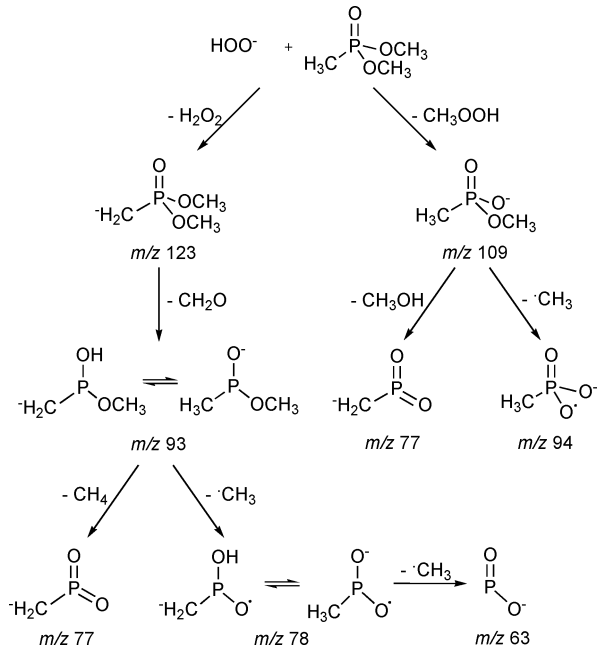

Scheme 4

loss of $^{\bullet}CH_3$, presumably to form the resonance-stabilised radical anion $[CH_3P(O)O]^{-\bullet}$. A minor neutral loss of 16 Da (CH_4) was also observed in the MS^4 spectrum to form the $[CH_2P(O)O]^-$ ion (m/z 77). Further, the radical anion at m/z 78, $[CH_3P(O)O]^{-\bullet}$ readily undergoes loss of 15 Da ($^{\bullet}CH_3$), in an MS^5 experiment (Fig. 6d), resulting in an ion at m/z 63 which corresponds to a resonance-stabilised closed shell anion, $[PO_2]^-$. The observed fragmentation pathways of the m/z 123 product ion are shown in Scheme 4. The combined MS^n data (Fig. 6) for the m/z 109 and m/z 123 product ions formed by reaction of HOO^- with neutral DMMP are consistent with the proposed structures (Scheme 3).

Summarising the experimental results, the nucleophilic addition–elimination reaction at phosphorus was observed for the F^- anion as evidenced by reactant anion addition with concomitant loss of CH_3OH. In addition, reaction of $[H_2O \cdots F^-]$ with DMMP yielded a product ion at m/z 143 consistent with a reactive pentavalent intermediate stabilised *via* neutral loss of H_2O. The major gas phase reactions of the HOO^- anion with DMMP are the S_N2(carbon) process and deprotonation. The HOO^- experiments provide no evidence for the addition–elimination reaction occurring *via* a pentavalent intermediate. The S_N2(carbon) pathway is more significant than deprotonation and contrasts reported reactions of anions with DMMP in the gas phase, whereby deprotonation dominated whenever the reaction channel was active.[13] The HOO^- and CD_3O^- anions have similar proton affinities, and therefore the marked differences in observed reaction products indicates an inherently greater nucleophilicity of the HOO^- anion compared to CD_3O^- anion.

Electronic structure calculations

The deprotonation, S_N2(carbon), addition–elimination and reductive elimination pathways (Scheme 2) for the reaction between HOO^- and DMMP were investigated using hybrid density functional theory. Optimised structures of pertinent stationary points on the B3LYP/6-31+G(d) potential energy surface for

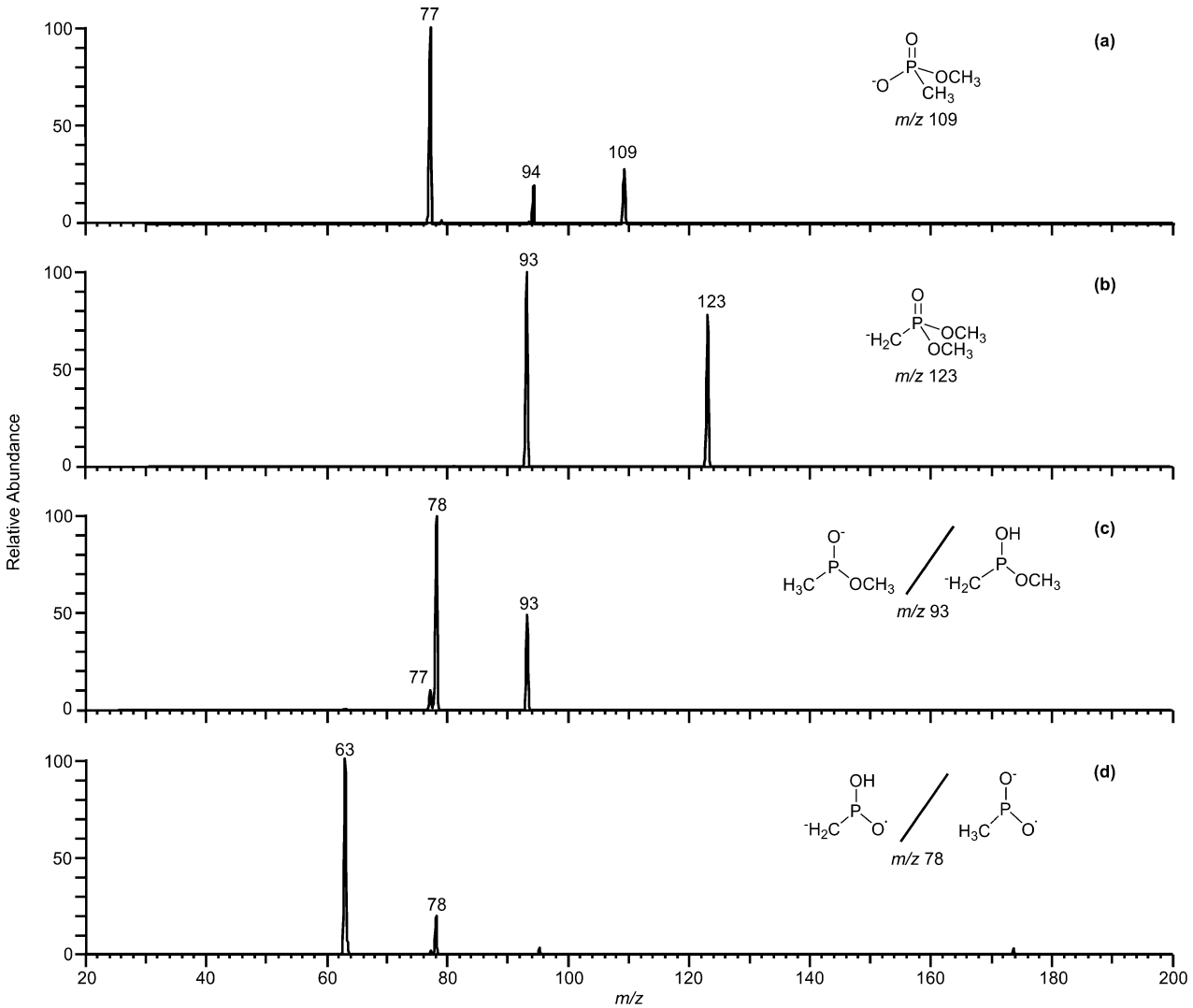

Fig. 6 MS^n spectra from $[DMMP - H]^-$ (m/z 123) formed by reaction with isolated HOO^- ion, namely (a) CID spectrum of m/z 109 (MS^3 of m/z 33 → 109), (b) CID spectrum of m/z 123 (MS^3 of m/z 33 → 123), (c) CID spectrum of the resulting fragment ion m/z 93 (MS^4 of m/z 33 → 123 → 93) and (d) CID spectrum of the resulting fragment ion m/z 78 (MS^5 of m/z 33 → 123 → 93 → 78).

each process are shown in Fig. 7, and the calculated energies, structural connectivity and transition state imaginary frequencies are detailed in Table 1. The conformation of DMMP (Fig. 7a) corresponds to the lowest energy conformation previously determined by Fourier transform microwave spectroscopy data.[20] The initial approach of the HOO^- anion for each reaction pathway considered was limited to one side of DMMP as indicated by the calculated structures for the reactant ion-neutral complex, RC1 (Fig. 7b) and the transition state for the S_N2(carbon) process, TS1 (Fig. 7c).

HOO^- reaction pathways observed: S_N2(carbon) and deprotonation. The dominant product ion (m/z 109) observed in the gas phase reaction between HOO^- and DMMP resulted from demethylation of DMMP by direct nucleophilic substitution at an ester carbon. This process was investigated at the B3LYP/aug-cc-pVTZ//B3LYP/6-31+G(d) level of theory (Fig. 8) and was calculated to be extremely exothermic for the formation of both the resulting product ion complex, PC1 (−258 kJ mol^{-1}), and separated products, CH_3O_2H and P1 (−186 kJ mol^{-1}). In addition, the process has a negative activation barrier, with the transition state TS1 calculated to be some 42 kJ mol^{-1} more stable than the isolated reactants (Table 1).

The reactant ion-neutral complex, RC1 (Fig. 7b), was calculated to be stabilised by 82 kJ mol^{-1} with respect to the separated reactants HOO^- and DMMP. The complex involves hydrogen bonding with the methyl and a methoxy group of DMMP with the charged oxygen centre of the incipient anion orientated for both deprotonation at the methyl group as well as nucleophilic addition at the phosphorus centre. Deprotonated DMMP was observed as a significant ion in the product ion mass spectrum of HOO^- reacting with neutral DMMP, and indicates a preference for the HOO^- anion to undergo deprotonation at the methyl group rather than nucleophilic addition at phosphorus. This proton transfer reaction was calculated to be a simple process with only one transition state leading directly to a product ion complex, PC2 (Fig. 8). The barrier for deprotonation was calculated to be 0.1 kJ mol^{-1} with respect to the pre-reactive complex RC1, and is therefore

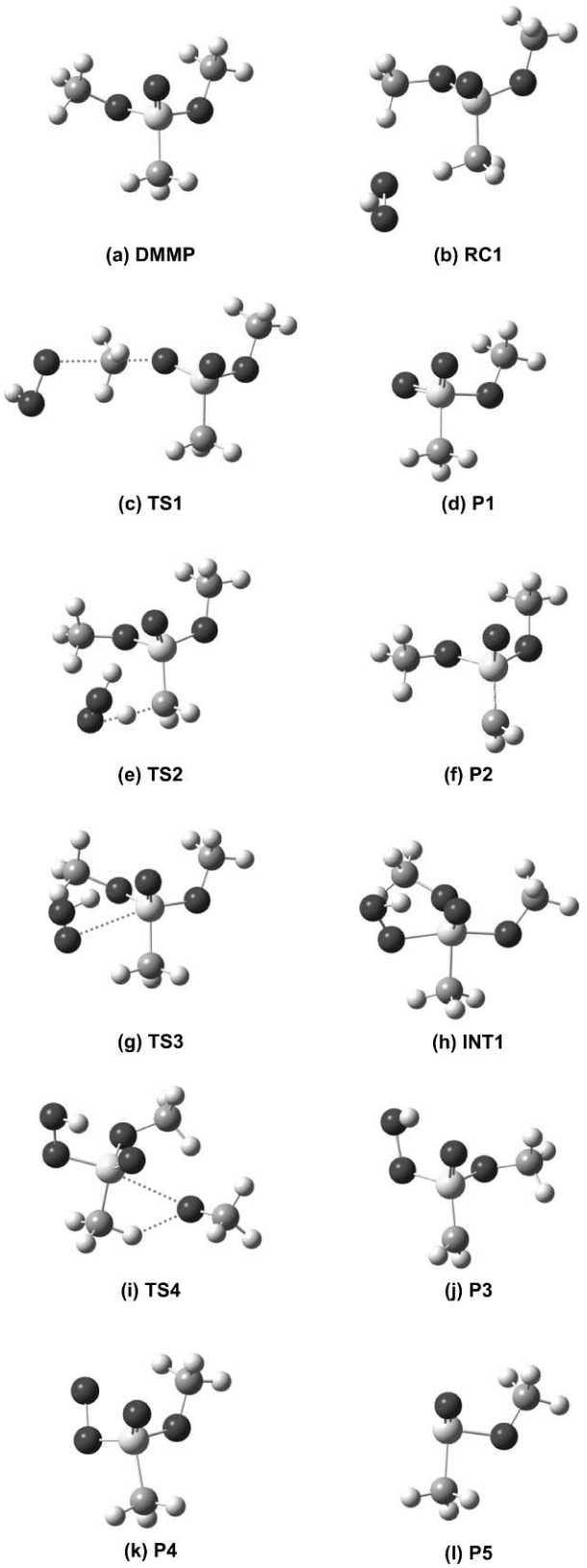

Fig. 7 Optimised geometries of pertinent stationary points on the B3LYP/6-31+G(d) potential energy surface for the gas phase reaction of HOO^- anion with DMMP. Standard orientations of all stationary points are provided in the supplementary data.

essentially barrierless. The energy required for dissociation of PC2 to form the observed product ion, P2 (90 kJ mol^{-1}, Fig. 7f), is less than the minimum excess internal energy of the system, but only 4 kJ mol^{-1} below the entrance channel.

HOO^- reaction pathways not observed: reductive elimination and addition–elimination. The addition–elimination process for the reaction between HOO^- and DMMP was also investigated using hybrid DFT calculations (Fig. 9). The initial attack was calculated to involve a specific orientation of the HOO^- anion with the charged oxygen atom directed toward the phosphorus atom and is stabilised by hydrogen bonding of the peroxyl hydrogen to the phosphonyl oxygen (TS3, Fig. 7g). A phosphorus-centred pentavalent intermediate (INT1, Fig. 7h) was calculated to be a stable stationary point on the potential energy surface. This intermediate was stabilised with respect to the initially formed reactant complex RC1 by 29 kJ mol^{-1} with a barrier to formation of 12 kJ mol^{-1}. Proceeding along the reaction coordinate, INT1 undergoes displacement of the opposing CH_3O group *via* a transition state, TS4 (Fig. 7i), similar to that of TS3. However, TS4 does not have a similar stabilising effect of hydrogen bonding at the reaction site and as a result has a significantly higher relative energy of 32 kJ mol^{-1} with respect to RC1. A CH_3O^- ion–neutral complex is not energetically stable on the potential energy surface and the departing CH_3O^- ion deprotonates the acidic phosphonyl methyl group to form a stable product ion–neutral complex, PC3 (−9 kJ mol^{-1}). This product ion complex is formed with a minimum of 91 kJ mol^{-1} of excess energy and can dissociate to yield the separated products, $[HOOP(O)(OCH_3)CH_2]^-$ (P3, Fig. 7j) and CH_3OH, with a relative energy 41 kJ mol^{-1} below the entrance channel. It should be noted that the product ion, P3, may undergo rearrangement to a more stable isomer, $[OOP(O)(OCH_3)CH_3]^-$ (P4, Fig. 7k), and stabilise the products by an additional 43 kJ mol^{-1} (Table 1).

Reductive elimination of DMMP has previously been observed only for the NH_2^- anion, and no experimental evidence for the process was observed during this study (Fig. 1). Calculations at the B3LYP/aug-cc-pVTZ//B3LYP/6-31+G(d) level of theory indicate that the reaction is significantly endothermic, with the relative energy of the products, $[CH_3P(O)OCH_3]^-$ (P5, Fig. 7l), CH_2O and H_2O_2, 144 kJ mol^{-1} above the pre-reactive complex, RC1 (Table 1). This energy requirement is 66 kJ mol^{-1} greater than the deprotonation process and therefore reductive elimination is not energetically competitive.

Entropy considerations. The theoretical data so far indicates that the addition–elimination reaction may proceed *via* a stable pentavalent intermediate ion. Further, the calculated excess energy of the system suggests that this process would result in the neutral loss of CH_3OH and formation of the product ion $[HOOP(O)(OCH_3)CH_2]^-$ at m/z 125. Despite these results, no direct experimental evidence was found for the formation of this ion in the gas phase. However, energetics alone are not sufficient to predict whether a particular reaction will be competitive or not. The rate of a reaction is also dependent on the Arrhenius pre-exponential factor. It has been demonstrated that for reactions occurring on the same potential energy surface comparison of the vibrational partition functions of pertinent transition states may provide insight into the relative values of the pre-exponential factors for each of the competing processes.[21,22] The vibrational

Table 1 Calculated data for selected stationary points on the B3LYP/6-31+G(d) potential energy surface for reaction between HOO^- and DMMP. Structures, zero point energies and imaginary frequencies were calculated at B3LYP/6-31+G(d). Relative energies were determined using the aug-cc-pVTZ basis set and include zero-point correction

Name	Chemical structure	Calculated energy/Hartrees	Zero point energy/Hartrees	Relative energy/kJ mol^{-1}
DMMP	$CH_3P(O)(OCH_3)_2$	−686.8877832	0.1288947	—
HOO^-	HOO^-	−150.9973058	0.0129208	—
HOO^- + DMMP	HOO^- + $CH_3P(O)(OCH_3)_2$	−837.885089	—	82.1
RC1	$[HOO\ CH_3P(O)(OCH_3)_2]^-$	−837.9163554	0.1429425	0.0
TS1 (−420 cm^{-1})	$[CH_3P(O)(OCH_3)O\cdot\cdot CH_3\cdot\cdot OOH]^-$	−837.9011263	0.1418708	40.0
PC1	$[CH_3P(O)(OCH_3)O\ CH_3OOH]^-$	−837.9835294	0.1450294	−176.4
P1	$CH_3P(O)(OCH_3)O^-$	−647.0718822	0.0878164	—
CH_3O_2H	CH_3OOH	−190.8840636	0.0546871	—
P1 + CH_3O_2H	$CH_3P(O)(OCH_3)O^-$ + CH_3OOH	−837.9559458	—	−103.9
TS2 (−970 cm^{-1})	$[HOO\cdot\cdot H\cdot\cdot CH_2P(O)(OCH_3)_2]^-$	−837.9162986	0.1393700	0.1
PC2	$[HOOH\ CH_2P(O)(OCH_3)_2]^-$	−837.9208791	0.1434266	−11.9
P2	$^-CH_2P(O)(OCH_3)_2$	−686.2951257	0.1135345	—
H_2O_2	$HOOH$	−151.5915359	0.0262686	—
P2 + H_2O_2	$^-CH_2P(O)(OCH_3)_2$ + $HOOH$	−837.8866616	—	78.0
TS3 (−92 cm^{-1})	$[HOO\cdot\cdot(CH_3)P(O)(OCH_3)_2]^-$	−837.9118082	0.1441214	11.9
INT1	$[HOO(CH_3)P(O)(OCH_3)_2]^-$	−837.9272842	0.1455452	−28.7
TS4 (−96 cm^{-1})	$[HOO(CH_3)P(O)(OCH_3)\cdot\cdot(OCH_3)]^-$	−837.9043289	0.1416032	31.6
PC3	$[HOO(CH_3O)P(O)CH_2\ HOCH_3]^-$	−837.9198117	0.1422469	−9.1
P3	$HOO(CH_3O)P(O)CH_2^-$	−722.1754949	0.0890622	—
CH_3OH	CH_3OH	−115.7253543	0.0512913	—
P3 + CH_3OH	$HOO(CH_3O)P(O)CH_2^-$ + CH_3OH	−837.9008492	—	40.7
P4	$^-OO(CH_3O)P(O)CH_3$	−722.1918917	0.0905185	—
P4 + CH_3OH	$^-OO(CH_3O)P(O)CH_3$ + CH_3OH	−837.9172460	—	−2.3
P5	$CH_3P(OCH_3)O^-$	−571.7448142	0.0817168	—
CH_2O	CH_2O	−114.525242	0.0267637	—
P5 + CH_2O	$CH_3P(OCH_3)O^-$ + CH_2O + $HOOH$	−837.8615921	—	143.8

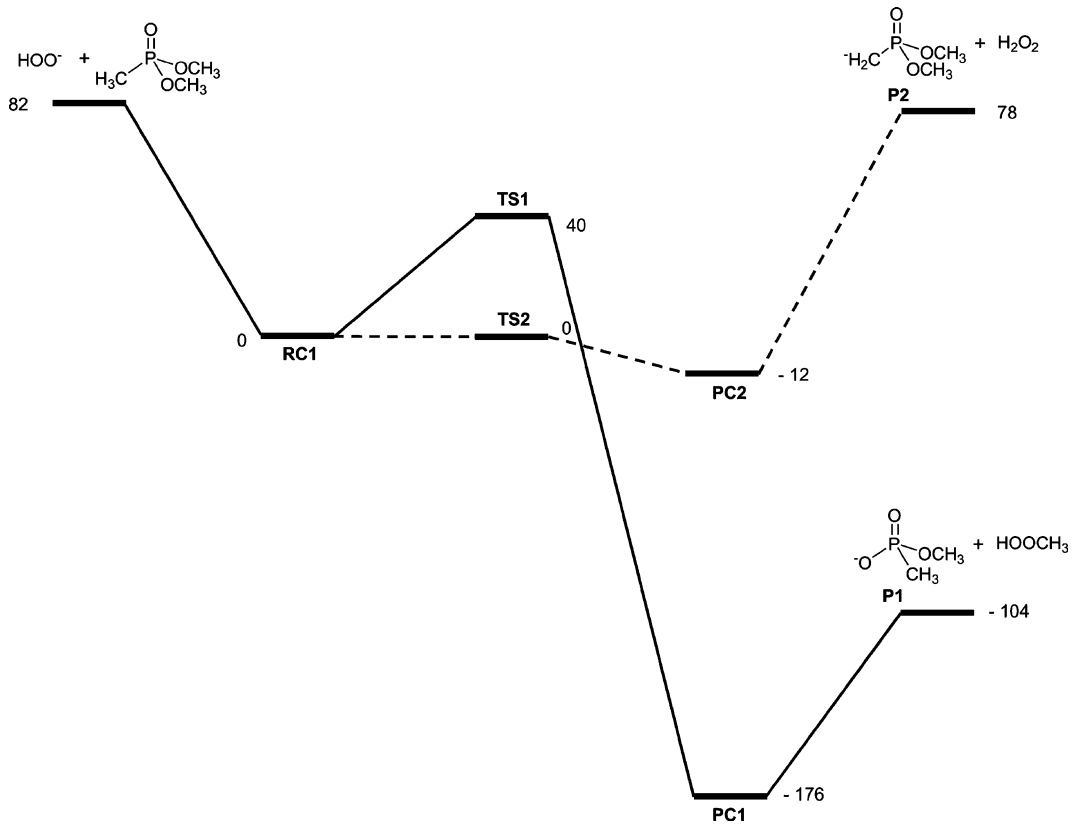

Fig. 8 Reaction coordinate diagram for the (a) S_N2(carbon) and (b) deprotonation processes observed during the gas phase reaction of HOO^- anion with DMMP in an ion trap. All structures were optimised at the B3LYP/6-31+G(d) level and energies calculated at the B3LYP/aug-cc-pVTZ//B3LYP/6-31+G(d) level.

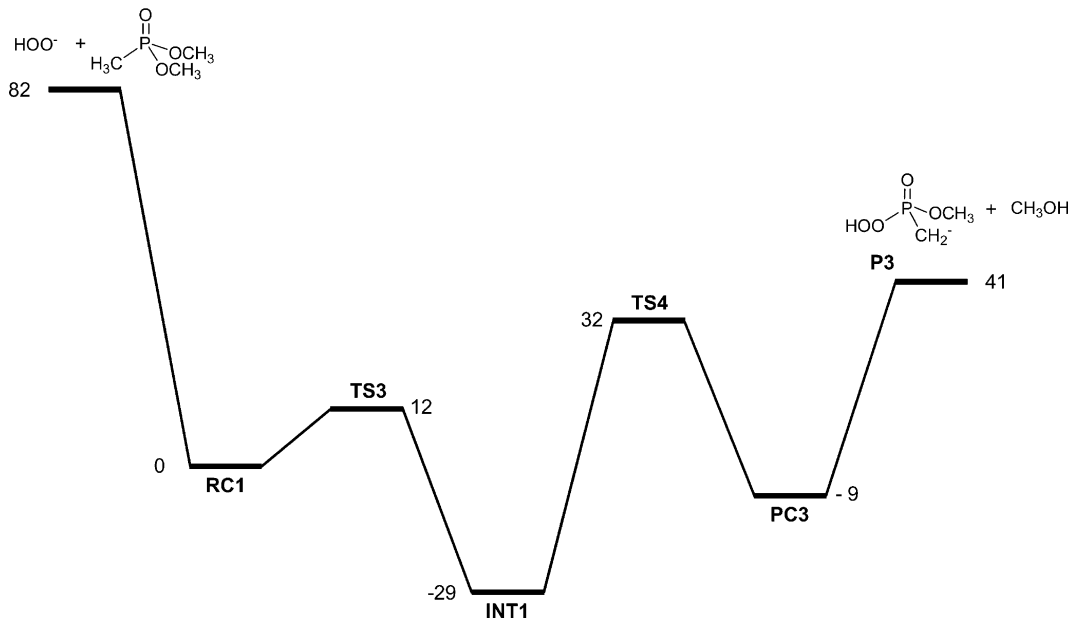

Fig. 9 Reaction coordinate diagram for the addition–elimination process which was not observed during the gas phase reaction of HOO^- anion with DMMP. All structures were optimised at B3LYP/6-31+G(d) level and energies calculated at the B3LYP/aug-cc-pVTZ//B3LYP/6-31+G(d) level.

partition function values were determined for the transition states TS1–TS3 (see ESI†). As previously reported,[21] there is a difficulty in knowing precisely which of the low frequency vibrations to use, but if all of the calculated frequencies are considered, the Arrhenius factor for the S_N2(carbon) process is twenty-seven times larger than that for the deprotonation pathway, which in turn is three times larger than the addition–elimination process (Table 2). This estimation of relative entropic contributions to the reaction rates is consistent with the S_N2(carbon) process being significantly more accessible as compared to the competing pathways. Further, the lower Arrhenius factor of the addition–elimination process relative to that of the deprotonation process explains the preference for deprotonation and absence of the addition–elimination process.

Thermodynamic considerations. The large dissociation energy of the product ion complex, PC2 (90 kJ mol^{-1}), relative to the reverse activation barrier (12 kJ mol^{-1}) indicates that the deprotonation process is readily reversible. Similarly, the reverse activation energy for the pentavalent intermediate, INT1 (41 kJ mol^{-1}), is less than the barrier of the forward process (61 kJ mol^{-1}), indicating that the addition–elimination process, if accessed, is also reversible. Conversely, the reverse activation barrier for PC1 (216 kJ mol^{-1}) is some three times greater than the energy required for dissociation (72 kJ mol^{-1}), indicating the S_N2(carbon) process is not readily reversible and proceeds directly to the separated products, P1 (m/z 109) and CH_3O_2H. Further, the S_N2(carbon) pathway is significantly exothermic (186 kJ mol^{-1}), as compared to the deprotonation (4 kJ mol^{-1}) and addition–elimination (41 kJ mol^{-1}) pathways, and explains the dominance of the S_N2(carbon) process in the reaction of HOO^- with DMMP.

The calculated α-effect of nucleophilic reactions. A number of pertinent stationary points for the reaction between CH_3O^- and DMMP were calculated at the B3LYP/aug-cc-pVTZ//B3LYP/6-31+G(d) level of theory to gain insight into the observed differences in the reactivity of CH_3O^- and HOO^- anions toward DMMP. Specifically, the reactant complex and first transition states for each of the analogous processes to that of the HOO^- anion were investigated and the results are listed in Table 3. There are no significant energetic or entropic differences between the deprotonation pathways of each anion. However, the activation energies of the S_N2(carbon) and addition–elimination processes were calculated to be significantly lower for HOO^- as compared to CH_3O^- (Table 2). Comparisons of nucleophiles of similar proton affinities have been suggested to provide a measure of the α-effect,[15] which in this case is calculated to be 7.8 kJ mol^{-1} for the S_N2(carbon) process and 18.2 kJ mol^{-1} for the nucleophilic addition–elimination process. In addition, the pre-exponential Arrhenius factors for the S_N2(carbon) and nucleophilic addition–elimination pathways, relative to the deprotonation pathway, are calculated to be appreciably larger for the reactions of

Table 2 Calculated activation energies and relative pre-exponential Arrhenius factors for reactions of HOO^- and CH_3O^- with DMMP

	HOO^-		CH_3O^-	
Reaction pathway	Activation energy/kJ mol^{-1}	Relative A factor	Activation energy/kJ mol^{-1}	Relative A factor
Deprotonation	0.1	1	1.2	1
S_N2(carbon)	40.0	27.4	47.8	9.7
Addition–elimination	11.9	0.3	30.1	0.2

Table 3 Calculated data for selected stationary points on the B3LYP/6-31+G(d) potential energy surface for reaction between CH_3O^- and DMMP. Structures, zero point energies and imaginary frequencies were calculated at B3LYP/6-31+G(d). Relative energies were determined using the aug-cc-pVTZ basis set and include zero point correction

Name	Chemical structure	Calculated energy/Hartrees	Zero point energy/Hartrees	Relative energy/kJ mol^{-1}
CH_3O^-	CH_3O^-	−115.1231623	0.0351421	—
CH_3O^- + DMMP	CH_3O^- + $CH_3P(O)(OCH_3)_2$	−802.0109455	—	80.2
RC2	$[CH_3O\ CH_3P(O)(OCH_3)_2]^-$	−802.041476	0.1660624	0.0
TS5 (−434 cm^{-1})	$[CH_3P(O)(OCH_3)O\cdot\cdot CH_3\cdot\cdot OCH_3]^-$	−802.0232846	0.1647602	47.8
CH_3OCH_3	CH_3OCH_3	−155.0129886	0.0800221	—
P1 + CH_3OCH_3	$CH_3P(O)(OCH_3)O^-$ + CH_3OCH_3	−802.0848708	—	−113.9
TS6 (−1019 cm^{-1})	$[CH_3O\cdot\cdot H\cdot\cdot CH_2P(O)(OCH_3)_2]^-$	−802.0410056	0.1624264	1.2
TS7 (−119 cm^{-1})	$[CH_3O\cdot\cdot(CH_3)P(O)(OCH_3)_2]^-$	−802.0300104	0.1666323	30.1
P2 + CH_3OH	$^-CH_2P(O)(OCH_3)_2$ + CH_3OH	−802.0204800	—	55.1

HOO^- compared to the analogous reactions of CH_3O^- (Table 2). Further, the pre-exponential Arrhenius factor is greatest for the S_N2(carbon) process involving HOO^- and is larger, relative to the deprotonation process, by a factor of twenty-seven. Based on these results, the addition–elimination process is significantly less competitive with respect to the S_N2(carbon) process for the HOO^- reaction with DMMP than that of CH_3O^-.

Experimental

Mass spectrometry

Experiments were performed on a modified ThermoFinnigan LTQ (San Jose, CA) linear quadrupole ion trap mass spectrometer[23] fitted with a conventional IonMax electrospray ionisation source and operating Xcalibur 2.0 SUR1 software. Ions were generated by infusion at 3–5 μL min^{-1} of an aqueous sample mixture (20 μM CsF or 10% H_2O_2), or neat methanol-d_4, into the electrospray ion source. Typical instrumental settings were: spray voltage −3.5 kV, capillary temperature 200–250 °C, sheath gas flow between 10–30 (arbitrary units), sweep and auxiliary gas flow set at between 0–10 (arbitrary units). For collision-induced dissociation (CID) experiments, ions were mass-selected with a window of 1–4 Da, using a *Q*-parameter of 0.250, and the fragmentation energy applied was typically 10–45 (arbitrary units) with an excitation time of 30 ms. Modifications to the mass spectrometer to allow the introduction of neutral gases into the ion trap region of the instrument have been previously described.[24] Briefly, neutral liquids and gases are introduced into a flow of ultra high purity (UHP) helium (3–5 psi) *via* a heated septum inlet (25–250 °C). The neutral flow is controlled using a syringe pump, while helium is supplied *via* a variable leak valve to provide a total ion gauge reading of ~0.9 × 10^{-5} Torr representing an estimated trap pressure of 2.5 mTorr. The temperature of the vacuum manifold surrounding the ion trap was measured at 307 ± 1 K, which is taken as being the effective temperature for ion–molecule reactions observed herein.[25] Reaction times of 0.03–200 ms were set using the excitation time parameter within the control software using a fragmentation energy of 0 (arbitrary units). All spectra presented represent are an average of at least 50 scans.

Dimethyl methylphosphonate (DMMP) and caesium fluoride were obtained from Sigma-Aldrich (Castle Hill, NSW, Australia). Aqueous hydrogen peroxide (50%) was obtained from APS Chemicals (Sydney, NSW, Australia). Methanol-d_4 (CD_3OD, 99.8% atom) was obtained from Cambridge Isotopes (Andover, MA, USA).

Electronic structure calculations

Geometry optimisations were carried out with the Becke 3LYP (B3LYP) method[26] using the 6-31+G(d) basis set within Gaussian 03 W suite of programs.[27] All stationary points were characterised as either minima (no imaginary frequencies) or transition states (one imaginary frequency) by calculation of the frequencies using analytical gradient procedures. Frequency calculations also provided zero-point energies, which were used to correct electronic energies calculated using the larger correlation consistent Dunnings basis set aug-cc-pVTZ.[28] The minima connected by a given transition state were confirmed by inspection of the animated imaginary frequency using the GaussView package[29] and by intrinsic reaction coordinate (IRC) calculation.[30]

Conclusions

The gas phase reactions of the HOO^- anion with neutral DMMP were investigated using a modified ion trap mass spectrometer. The major reaction product ions observed at *m/z* 109 and *m/z* 123 were the result of S_N2(carbon) and deprotonation processes, respectively. MS^n experiments carried out on the observed product ions support the structural assignment of $[CH_3P(O)(OCH_3)O]^-$ (*m/z* 109) and $[CH_2P(O)(OCH_3)_2]^-$ (*m/z* 123). The addition–elimination reaction occurring *via* a pentavalent intermediate was not observed for HOO^-. However, this pathway was observed to a minor extent for the reaction of F^- with DMMP. Further, reactions of $[H_2O\cdots F^-]$ with DMMP provides evidence for the elusive pentavalent intermediate $[F(CH_3)P(O)(OCH_3)_2]^-$ (*m/z* 143). In contrast, the gas phase reactions of CD_3O^- with DMMP were dominated by deprotonation, with the S_N2(carbon) process only occurring to a minor extent. Since HOO^- and CD_3O^- have similar proton affinities the marked difference in observed branching ratios is a result of an inherently greater nucleophilicity of the HOO^- anion. Thus, the work herein describes the first experimental evidence of an α-effect in the gas phase.

Hybrid DFT calculations, at the B3LYP/aug-cc-pVTZ//B3LYP//6-31+G(d) level, were used to investigate the mechanisms of the observed processes. The S_N2(carbon) process was calculated to be exothermic by 186 kJ mol^{-1} and compared to the deprotonation process which was calculated to be exothermic only by 4 kJ mol^{-1}. The observed branching ratios for the S_N2(carbon) (89%) and deprotonation (11%) are

a result of the significant difference in reaction exothermicities. The reaction pathway for the addition–elimination process was also calculated using the hybrid DFT method and the process determined to be exothermic by 41 kJ mol^{-1}. However, an estimation of the relative Arrhenius pre-exponential factors of the initial transition states of the three pathways investigated indicate that the addition–elimination is not kinetically competitive. In addition, the S_N2(carbon) process is readily accessible and extremely exothermic and explains the pathways dominance in the reaction of HOO^- and DMMP.

The observation of a gas phase α-effect for the hydroperoxide anion indicate that mass spectrometry can be used to investigate the intrinsic chemistry of CWA perhydrolysis. In the case of DMMP, the phosphorus-centred pathway was not observed and therefore this system may not be a suitable to probe the perhydrolysis degradation of CWAs which differ by the presence of P–F or P–S bonds and larger alkyl groups. These results highlight the importance of the electrophilicity at phosphorus, bonding at phosphorus, steric and solvent effects in the study of CWAs and their simulants.

Acknowledgements

The authors would like to thank Dr David Harman (UoW) for technical assistance and the Australian Partnership for Advanced Computing (ANU, Canberra) for a generous allocation of super-computing time. AMM acknowledges the honorary position of Visiting Senior Fellow at UoW and a DSTO Fellowship Award which generously supported this project. SJB acknowledges an ARC grant (DP0452849) and thanks UoW and DSTO for their support.

References

1 L. M. Eubanks, T. J. Dickerson and K. D. Janda, *Chem. Soc. Rev.*, 2007, **36**, 458–470; B. C. Giordano and G. E. Collins, *Curr. Org. Chem.*, 2007, **11**, 255–265; S. S. Talmage, A. P. Watson, V. Hauschild, N. B. Munro and J. King, *Curr. Org. Chem.*, 2007, **11**, 285–298; J. P. Fitch, E. Raber and D. R. Imbro, *Science*, 2003, **302**, 1350–1354; B. K. Singh and A. Walker, *FEMS Microbiol. Rev.*, 2006, **30**, 428–471; Y. C. Yang, *Acc. Chem. Res.*, 1999, **32**, 109–115; Y. C. Yang, J. A. Baker and J. R. Ward, *Chem. Rev.*, 1992, **92**, 1729–1743.
2 J. Epstein, M. M. Demek and D. H. Rosenblatt, *J. Org. Chem.*, 1956, **21**, 796–797; Y. C. Yang, *Chem. Ind.*, 1995, 334–337.
3 Y. C. Yang, L. L. Szafraniec, W. T. Beaudry and D. K. Rohrbaugh, *J. Am. Chem. Soc.*, 1990, **112**, 6621–6627; Y. C. Yang, L. L. Szafraniec, W. T. Beaudry and C. A. Bunton, *J. Org. Chem.*, 1993, **58**, 6964–6965.
4 Y. C. Yang, F. J. Berg, L. L. Szafraniec, W. T. Beaudry, C. A. Bunton and A. Kumar, *J. Chem. Soc., Perkin Trans. 2*, 1997, 607–613.
5 G. W. Wagner and Y. C. Yang, *Ind. Eng. Chem. Res.*, 2002, **41**, 1925–1928.
6 G. W. Wagner, D. C. Sorrick, L. R. Procell, M. D. Brickhouse, L. F. McVey and L. I. Schwartz, *Langmuir*, 2007, **23**, 1178–1186.
7 D. E. Richardson, H. Yao, K. M. Frank and D. A. Bennett, *J. Am. Chem. Soc.*, 2000, **122**, 1729–1739.
8 J. O. Edwards and R. G. Pearson, *J. Am. Chem. Soc.*, 1962, **84**, 16–24.
9 E. V. Patterson and C. J. Cramer, *J. Phys. Org. Chem.*, 1998, **11**, 232–240.
10 J. Seckute, J. L. Menke, R. J. Emnett, E. V. Patterson and C. J. Cramer, *J. Org. Chem.*, 2005, **70**, 8649–8660.
11 F. Zheng, C. G. Zhan and R. L. Ornstein, *J. Chem. Soc., Perkin Trans. 2*, 2001, 2355–2363.
12 Y. Song and R. G. Cooks, *J. Mass Spectrom.*, 2007, **42**, 1086–1092; T. Faye, J. C. Mathurin, A. Brunot, J. C. Tabet, G. Walls and C. Fuche, *Anal. Chem.*, 2000, **72**, 5063–5069; V. Steiner, I. Daoust-Maleval and J. C. Tabet, *Int. J. Mass Spectrom.*, 2000, **195–196**, 121–138; R. C. Lum and J. J. Grabowski, *J. Am. Chem. Soc.*, 1992, **114**, 8619–8627; R. V. Hodges, T. J. McDonnell and J. L. Beauchamp, *J. Am. Chem. Soc.*, 1980, **102**, 1327–1332; R. V. Hodges, S. A. Sullivan and J. L. Beauchamp, *J. Am. Chem. Soc.*, 1980, **102**, 935–938.
13 R. C. Lum and J. J. Grabowski, *J. Am. Chem. Soc.*, 1993, **115**, 7823–7832.
14 C. H. DePuy, E. W. Della, J. Filley, J. J. Grabowski and V. M. Bierbaum, *J. Am. Chem. Soc.*, 1983, **105**, 2481–2482.
15 Y. Ren and H. Yamataka, *Org. Lett.*, 2006, **8**, 119–121; Y. Ren and H. Yamataka, *J. Org. Chem.*, 2007, **72**, 5660–5667; Y. Ren and H. Yamataka, *Chem. Eur. J.*, 2007, **13**, 677–682.
16 T. M. Ramond, S. J. Blanksby, S. Kato, V. M. Bierbaum, G. E. Davico, R. L. Schwartz, W. C. Lineberger and G. B. Ellison, *J. Phys. Chem. A*, 2002, **106**, 9641–9647.
17 T. M. Ramond, G. E. Davico, R. L. Schwartz and W. C. Lineberger, *J. Chem. Phys.*, 2000, **112**, 1158–1169.
18 C. Blondel, C. Delsart and F. Goldfarb, *J. Phys. B: At. Mol. Opt. Phys.*, 2001, **34**.
19 J. J. Grabowski and R. C. Lum, *J. Am. Chem. Soc.*, 1990, **112**, 607–620.
20 R. D. Suenram, F. J. Lovas, D. F. Plusquellic, A. Lesarri, Y. Kawashima, J. O. Jensen and A. C. Samuels, *J. Mol. Spectrom.*, 2002, **211**, 110–118.
21 A. M. McAnoy, S. Dua, S. J. Blanksby and J. H. Bowie, *J. Chem. Soc., Perkin Trans. 2*, 2000, 1665–1673.
22 J. M. Hevko, S. Dua, J. H. Bowie and M. S. Taylor, *J. Chem. Soc., Perkin Trans. 2*, 1999, 457–464.
23 J. C. Schwartz, M. W. Senko and J. E. P. Syka, *J. Am. Soc. Mass Spectrom.*, 2002, **13**, 659–669.
24 D. G. Harman and S. J. Blanksby, *Org. Biomol. Chem.*, 2007, **5**, 3495–3503.
25 S. Gronert, *J. Am. Soc. Mass Spectrom.*, 1998, **9**, 845–848.
26 A. Becke, *J. Chem. Phys.*, 1993, **98**, 1372–1377; C. T. Lee, W. T. Yang and R. G. Parr, *Phys. Rev. B*, 1988, **37**, 785–789.
27 M. J. Frisch, G. W. Trucks, H. B. Schlegel, G. E. Scuseria, M. A. Robb, J. R. Cheeseman, J. A. Montgomery, Jr., T. Vreven, K. N. Kudin, J. C. Burant, J. M. Millam, S. S. Iyengar, J. Tomasi, V. Barone, B. Mennucci, M. Cossi, G. Scalmani, N. Rega, G. A. Petersson, H. Nakatsuji, M. Hada, M. Ehara, K. Toyota, R. Fukuda, J. Hasegawa, M. Ishida, T. Nakajima, Y. Honda, O. Kitao, H. Nakai, M. Klene, X. Li, J. E. Knox, H. P. Hratchian, J. B. Cross, V. Bakken, C. Adamo, J. Jaramillo, R. Gomperts, R. E. Stratmann, O. Yazyev, A. J. Austin, R. Cammi, C. Pomelli, J. Ochterski, P. Y. Ayala, K. Morokuma, G. A. Voth, P. Salvador, J. J. Dannenberg, V. G. Zakrzewski, S. Dapprich, A. D. Daniels, M. C. Strain, O. Farkas, D. K. Malick, A. D. Rabuck, K. Raghavachari, J. B. Foresman, J. V. Ortiz, Q. Cui, A. G. Baboul, S. Clifford, J. Cioslowski, B. B. Stefanov, G. Liu, A. Liashenko, P. Piskorz, I. Komaromi, R. L. Martin, D. J. Fox, T. Keith, M. A. Al-Laham, C. Y. Peng, A. Nanayakkara, M. Challacombe, P. M. W. Gill, B. G. Johnson, W. Chen, M. W. Wong, C. Gonzalez and J. A. Pople, *GAUSSIAN 03 (Revision D.01)*, Gaussian, Inc., Wallingford, CT, 2004.
28 D. E. Woon and T. H. Dunning Jr, *J. Chem. Phys.*, 1993, **98**, 1358–1371.
29 R. Dennington, II, T. Keith, J. Millam, K. Eppinnett, W. L. Hovell and R. Gilliland, *GaussView, Version 4.1*, Semichem, Inc., Shawnee Mission, KS, 2003.
30 C. Gonzalez and H. B. Schlegel, *J. Chem. Phys.*, 1989, **90**, 2154–2161; C. Gonzalez and H. B. Schlegel, *J. Phys. Chem.*, 1990, **94**, 5523–5527.

